The Journal of Medicinal Plants and By-products

Original Article

Biosynthesis of Silver Nanoparticles Using Oleander (*Nerium oleander*) Extract and Its Effect on the Expression of the *TEM* Gene in *Escherichia coli* Causing urinary tract infections

Nahid Heydari[1], Zeinab Fotoohiyan[2], Mohammad shariati[3], Ali Salehi Sardoei[4], Reza Ghasemi[5], Hamidreza Balouchi[6] and Bahman Fazeli-Nasab[7*]

[1] *Department of Microbiology Plant Pathology, Ji.c., Islamic Azad University, Jiroft, Iran*
[2] *Department of Plant Pathology, Ji.c., Islamic Azad University, Jiroft, Iran*
[3] *Jiroft Social Security Clinic, Jiroft, Iran*
[4] *Crop and Horticultural Science Research Department, South Kerman Agricultural and Natural Resources Research and Education Center, Agricultural Research, Education and Extension Organization (AREEO), Jiroft, Iran*
[5] *Department of Environmental Health Engineering, Tehran University of Medical Science, Tehran, Iran*
[6] *Agronomy and Plant Breeding Department, Faculty of Agriculture, Yasouj University, Yasouj, Iran*
[7] *Department of Agronomy and Plant Breeding, Agriculture Institute, Research Institute of Zabol, Zabol, Iran*

*Corresponding Author: Email: fazelinsb@rizabol.ac.ir

Article History: Received 22 February 2026/Accepted in revised form 04 September 2026

ABSTRACT

E. coli's *TEM* gene-mediated resistance to beta-lactams challenges UTI treatment. This study explores oleander-synthesized silver nanoparticles as a novel antimicrobial strategy against resistant strains. To assess *TEM* gene prevalence in *E. coli* isolates and evaluate oleander-based AgNPs and methyltransferase interactions for combating antibiotic resistance. A total of 155 UTI-associated *E. coli* isolates were identified via biochemical tests and ESBL screening (CLSI guidelines). *TEM* gene detection used PCR with specific primers. Oleander-synthesized AgNPs were characterized (UV-Vis) and tested for antimicrobial activity (disk diffusion, MIC/MBC). Protein-protein docking analyzed *blaTEM* (KX462012.1) and oleander methyltransferase (MH504111.1) interactions. Experimental data analyzed via randomized ANOVA, Duncan's test ($p<0.05$), PFAFFL. Among 155 *E. coli* isolates from UTIs, 65% (100 strains) produced ESBLs, with highest resistance to ampicillin (74%), carbenicillin (61%), and chloramphenicol (53%). PCR confirmed the *blaTEM* gene in 60% of tested isolates. Oleander-synthesized silver nanoparticles (AgNPs) exhibited potent antimicrobial activity, showing dose-dependent inhibition zones (10–40 µg/mL), with MIC and MBC values of 16 µg/mL and 32 µg/mL, respectively. Real-time PCR revealed a 48.5% reduction in *blaTEM* expression (*p* < 0.05) after AgNP treatment. Molecular docking demonstrated stable binding between *blaTEM* and oleander methyltransferase, driven by hydrophobic interactions (Leu, Ile, Val, Phe, Trp), with Trp playing a pivotal role. Ramachandran plots validated high-quality 3D structures (94–96% favored residues) for both proteins. The study isolated 155 *E. coli* strains (65% ESBL-producing) from UTIs, showing high antibiotic resistance. Oleander-synthesized silver nanoparticles (MIC: 16 µg/mL) inhibited *TEM* gene-carrying *E. coli* and reduced *TEM* expression by 48.5%. Oleander methyltransferase stably binds *blaTEM* via hydrophobic interactions, validated by high-quality 3D modeling and docking studies.

Keywords: *Escherichia coli*, *Nerium oleander*, *ESBL*, *TEM* gene, In Silico

INTRODUCTION

Escherichia coli (*E. coli*) stands as one of the leading causes of human infections which result in urinary tract infections (UTIs), gastrointestinal infections and neonatal meningitis [1, 2]. This Gram-negative pathogen develops resistance to beta-lactam antibiotics and broad-spectrum cephalosporins through the acquisition of plasmids that produce extended-spectrum beta-lactamases (ESBL). Consequently, the bacterium's resistance to beta-lactam antibiotics makes treatment of its infections challenging according to Bhattacharjee *et al*. [3]. The beta-lactam antibiotics which comprise penicillins, cephalosporins and monobactams target transpeptidases through binding to penicillin-binding proteins (PBPs) in bacterial cell walls which interrupts peptidoglycan synthesis and causes bacterial death.

The synthesis of beta-lactamase enzymes is the main cause of bacterial resistance to beta-lactam antibiotics, which hydrolyze the antibiotics before they can reach their intended PBPs [4]. The *TEM* gene represents more than 90% of beta-lactamase types responsible

for *E. coli* resistance to ampicillin according to research by Jacoby and Medeiros [5]. Scientists first isolated the *TEM* enzyme from an *E. coli* strain taken from the blood culture of a Greek patient named *Temoniera* who lent his name to the enzyme [6]. Researchers have discovered more than 130 *TEM* enzyme variants which show differences in their active site amino acid sequences [7]. Infections from bacteria that produce plasmid-mediated *ESBLs* pose great difficulty to treat and create a major clinical obstacle [8]. The global increase in UTIs correlates with the dissemination of resistant bacteria while highlighting the necessity for antibiotic susceptibility evaluations and research into the *TEM beta-lactamase* gene present in *E. coli* urinary isolates.

A recent global surge in antibiotic resistant bacterial infections shows an increase rate between 42% and 100% [9]. The *ESBL* enzymes destroy beta-lactam antibiotics' core structure which makes them ineffective [10]. The genes that produce *ESBL* enzymes mainly reside on plasmids which enable resistance to multiple antibiotic classes thus complicating treatment choices [11]. *E. coli* and *Klebsiella pneumoniae* commonly express *ESBL TEM* beta-lactamases where TEM-1 accounts for more than 90% of *E. coli* resistance to ampicillin while hydrolyzing penicillins and first-generation cephalosporins such as cephalothin and cephaloridine [12].

The molecular identification of *ESBL*-producing genes like *TEM*, *SHV*, and *CTX-M* together with antibiotic resistance pattern evaluations generates essential epidemiological data needed for proper antimicrobial treatment according to Geyer and Hanson [13]. While phenotypic tests fail to differentiate between various *ESBL* enzyme producing strains, molecular methods deliver exact identification of antibiotic resistance genes at greater expense. Studies in Tehran by Hosseini-Mazinani *et al*. [14] alongside Masjedian *et al*. [15] who conducted studies in Isfahan, disclosed *E. coli* isolates exhibited *TEM* gene frequencies of 60% and 84.6%, respectively.

Research dating back to Allafchian *et al*. [16] has long identified silver as an antimicrobial agent. Silver nanoparticles (AgNPs) sized between 1 and 100 nm attach to sulfur-rich proteins in bacterial membranes which leads to changes in membrane shape and function as well as disruptions in respiratory processes and cell replication resulting in bacterial death. AgNPs possess distinctive physical, chemical and biological characteristics that enable antibacterial, antioxidant and anticancer functions [17]. Scientific reports have confirmed that AgNPs show antimicrobial effectiveness by interrupting bacterial metabolism along with their respiratory processes and cell reproduction functions [18].

In recent years, the applications of nanotechnology have expanded rapidly across various biomedical and biotechnological fields. Novel nanocarriers, such as nanoliposomes, have been developed to improve the local delivery and stability of active biomolecules [19], while incorporating nanoparticles into polymeric hydrogels has emerged as a key strategy to reinforce wound healing structures and enhance their physical and biological properties [20]. Furthermore, functionalized and hybrid metal/metal-oxide nanoparticles—such as functionalized magnetic silica systems or silver–cerium oxide nanocomposites—have demonstrated outstanding potential in stabilizing bioactive agents and improving target utilization in agricultural systems [21, 22]. Similarly, nano-encapsulation techniques using polymeric or lipid shells have successfully protected essential oils and plant secondary metabolites to elicit disease resistance and fight pathogens [23].

The biosynthetic production of AgNPs from herbal extracts attracts many researcher attentions because of their eco-friendly nature, affordability, non-toxic properties, and superior purity [24, 25]. Secondary plant metabolites like flavonoids, phenolics, proteins, enzymes, carbohydrates and lipids enable the conversion of Ag^+ ions into AgNPs. Recent studies demonstrated that plant extracts from *Aloe vera*, *Artemisia afra*, elderberry, orange blossom, and marjoram exhibited significant antimicrobial effects against hospital-acquired infections according to Chahardooli and Khodadadi [26].

Oleander (*N. oleander*) belongs to the Mediterranean region and grows as a toxic perennial evergreen shrub that people cultivate in landscapes as an ornamental plant [27]. Extracts from oleander demonstrate therapeutic properties, including anti-inflammatory effects and anticancer activities, despite containing toxic cardiac glycosides [28]. Considering Iran's rich biodiversity combined with oleander's proven therapeutic benefits makes it vital to find new antimicrobial agents that fight bacterial resistance with fewer side effects. Oleandrin is a cardiac glycoside primarily derived from the oleander plant (*N. oleander*). Its structure features a steroid nucleus with an unsaturated lactone ring at C17, a dideoxy arabinose group at C3, and an acetyloxy substitution at C16. While oleandrin's structure is similar to that of digoxin and ouabain, it is less potent than digoxin but more potent than ouabain. As a lipophilic compound, oleandrin inhibits the Na^+/K^+ ATPase pump, disrupting cellular ion balance and increasing intracellular calcium levels. This mechanism contributes to its cardiotoxic effects and its historical use in traditional medicine for conditions like heart failure. However, despite anecdotal claims, there is no clinical evidence supporting its safety or efficacy, and it lacks regulatory approval [29].

Studies on the antimicrobial effects of oleandrin against *E. coli* yield conflicting results. Chloroform and petroleum ether extracts of *N. oleander* leaves have shown inhibitory activity against *E. coli in vitro*, while aqueous and ethanolic extracts have not affected standard *E. coli* strains in other experiments. This discrepancy may be attributed to differences in extraction methods or compound concentrations. For instance, one study reported moderate antibacterial activity against *E. coli* using methanolic extracts, whereas another study found that *E. coli* was resistant to both aqueous and ethanolic extracts. Additionally, the limited bioavailability of oleandrin and its derivatives in systemic circulation complicates their potential therapeutic use against bacterial infections [30, 31].

The variability in oleandrin's antibacterial efficacy underscores the necessity for standardized research methodologies. Some studies indicate that Gram-negative bacteria, such as *E. coli*, might develop resistance due to their impermeable cell envelopes. In contrast, other research suggests potential synergistic effects when oleandrin-containing extracts are combined with antibiotics like ceftriaxone. Nevertheless, the compound's high toxicity, slow clearance, and accumulation in critical organs, including the heart and liver, outweigh its unproven antimicrobial advantages. Current evidence does not support its use in clinical or dietary applications, highlighting the risks linked to its unregulated consumption [30, 32, 29].

Oleander methyltransferase mRNA encodes enzymes that facilitate the methylation of various secondary metabolites, such as Oleandrin, in the oleander plant (*N. oleander*). Methyltransferases are crucial for the biosynthesis and modification of plant-derived compounds, many of which exhibit antimicrobial properties. By catalyzing the transfer of methyl groups to specific substrates, these enzymes can modify the biological activity, solubility, and stability of phytochemicals, potentially increasing their effectiveness in inhibiting microbial growth [30, 33].

While direct studies on the specific antimicrobial role of oleander methyltransferase mRNA are limited, existing literature suggests that plant methyltransferases play a significant role in producing bioactive metabolites with antibacterial properties. For instance, methylated alkaloids and flavonoids generated by these enzymes have shown effectiveness against multidrug-resistant bacteria, such as *E. coli* and *Staphylococcus aureus* (*S. aureus*). These compounds can disrupt bacterial cell division, inhibit biofilm formation, and interfere with vital cellular processes, thereby preventing microbial growth [33]. Various phenolic and flavonoid compounds found in *N. oleander* extracts, likely resulting from methyltransferase activity, have been linked to significant antibacterial effects against both Gram-positive and Gram-negative bacteria, including *E. coli* [29]. Recent experimental studies have confirmed the antimicrobial potential of *N. oleander* leaf extracts, which are abundant in methylated secondary metabolites. These extracts have demonstrated inhibitory effects on the growth of *E. coli*, with minimum inhibitory concentrations (MIC) reaching as low as 12.5 µg/mL in some investigations. The antibacterial activity is attributed to the synergistic action of various phytochemicals, many of which are modified by methyltransferases. This highlights the significance of oleander methyltransferase mRNA in the plant's natural defense against microbial pathogens [33, 29].

This study sought to determine the frequency of the *blaTEM* gene among *E. coli* urinary isolates obtained over a one-year period from Dr. Shariati Laboratory. To the best of our knowledge, this work is the first in Iran to investigate the antibacterial efficacy of *Nerium oleander*-derived silver nanoparticles against *blaTEM*-positive *E. coli* isolates. Furthermore, to elucidate the molecular mechanisms of inhibition, in silico molecular docking was conducted to evaluate the binding interactions between the *TEM* beta-lactamase enzyme from *Escherichia coli* (derived from GenBank: KX462012.1) and key bioactive secondary metabolites of *N. oleander*—specifically those synthesized via the oleander methyltransferase pathway (GenBank: MH504111.1)—acting as potential inhibitors."

MATERIALS AND METHODS

Isolation and Identification of *E. coli* Strains Causing UTIs

The diagnostic laboratory in Jiroft County obtained 155 urine samples from patients diagnosed with UTIs throughout 2023 and 2024. The identification of bacterial samples followed the standard Enterobacteriaceae microbiological testing procedures which involved Gram staining and biochemical tests such as catalase and urease tests, hydrogen sulfide production, carbohydrate fermentation, and nitrate reduction after growing cultures on selective and differential media. The differential media used in this study were Triple Sugar Iron (TSI) agar, Simmons Citrate Agar, Sulfide Indole Motility (SIM) medium, Methyl Red/Voges-Proskauer (MR/VP) broth, and Eosin Methylene Blue (EMB) agar. The biochemical identification was validated using the IMViC tests, matching the outcomes with established standard references. The SIM medium provided analysis results for motility, indole production, and hydrogen sulfide generation. Antibiogram testing utilized Mueller-Hinton Broth and Mueller-Hinton Agar, while isolates were stored for later evaluation in Tryptic Soy Broth (TSB) containing 15% glycerol at –20 °C.

Beta-lactamase Production by *E. coli* Isolates

The frozen *E. coli* samples were brought to room temperature before being cultured onto MacConkey and EMB agars and then incubated at 37 °C overnight. The double-disk synergy (DDS) test, based on the Clinical and Laboratory Standards Institute (CLSI) guidelines, was performed to screen for *ESBL*-producing strains by Jacoby and Medeiros [5]. Briefly, Mueller-Hinton Agar plates were prepared, and bacterial suspensions were adjusted to a 0.5 McFarland standard (1.5×10^8 CFU/mL) before creating lawn cultures using sterile swabs. The agar surface received disks containing ceftazidime (30 µg), ceftazidime-clavulanic acid (30/10 µg), cefotaxime (30 µg), and cefotaxime-clavulanic acid (30/10 µg) (Mast, UK) positioned at a distance of 25 mm (center-to-center). The plates were incubated at 37 °C for 24 h. Isolates were classified as *ESBL*-positive when the ceftazidime-clavulanate inhibition zone exceeded that of ceftazidime by ≥5 mm, or when the cefotaxime-clavulanate zone surpassed the cefotaxime zone by ≥3 mm.

Antibiotic Susceptibility Testing

The disk diffusion method (Kirby–Bauer) on Mueller-Hinton Agar was employed to determine antibiotic susceptibility patterns. Antibiotic disks (Padtan Teb, Iran) contained carbenicillin (100 µg), penicillin (25 µg), ampicillin (10 µg), ofloxacin (5 µg), streptomycin (10 µg), tetracycline (30 µg), chloramphenicol (30 µg), nitrofurantoin (300 µg), norfloxacin (10 µg), and ciprofloxacin (5 µg). Each isolated sample received a 0.5 McFarland suspension before being lawn-inoculated onto Mueller-Hinton Agar. After a 10–15 min room temperature stabilization period, the antibiotic disks were applied to the agar surface at 1.5 cm from the edge and spaced 2.5 cm apart. The plates underwent incubation at 37 °C for 18 to 24 h before measuring the zones of inhibition. CLSI guidelines served as the standard for determining susceptibility and resistance.

Preparation of *N. oleander* Extract

Nerium oleander leaves collected from Jiroft and Anbarabad regions underwent taxonomic verification at the Faculty of Pharmacy, Kerman University of Medical Sciences. An aqueous extract was prepared through the maceration of dried leaves. The leaves were dried under shaded conditions at room temperature (25 ± 2 °C) and pulverized into a fine powder. Five hundred grams of the powder was boiled in 1000 mL of double-distilled water for 10 min. After initial filtration through Whatman No. 1 filter paper, the extract was centrifuged at 4000 rpm for 20 min to eliminate residual suspended particles. The supernatant was stored at 4 °C awaiting future experimental use as described by Hashemi *et al*. [34].

Biosynthesis and Characterization of Silver Nanoparticles (AgNPs)

For the biosynthesis of AgNPs, 30 mL of the aqueous leaf extract was mixed with 90 mL of a freshly prepared 1 mM silver nitrate (AgNO3, Sigma-Aldrich) solution. The reaction mixture was maintained at 40 °C under pH 8 in complete darkness to prevent photo-reduction. A control sample containing only the plant extract without AgNO3 was maintained under identical conditions. The transition of the solution from pale yellow to dark brown after 24 h served as a visual indicator of AgNP formation.

To comprehensively characterize the green-synthesized AgNPs, the following analyses were conducted:

UV-Visible Spectroscopy: The bioreduction of Ag+ ions was monitored using a UV-Vis spectrophotometer (Double Beam, Shimadzu) in the wavelength range of 300 to 650 nm [35, 36].

Identification of *E. coli* Carrying the *TEM* Gene Using PCR

The DNA extraction process followed the protocol outlined by the Kia Gene DNA kit. Multiplex PCR was performed using a primer pair targeting the *blaTEM* gene (Table 1). Ten isolates from the 100 beta-lactamase-positive samples were grown in 5 mL of TSB medium at 37 °C for 16–18 h. The pellet obtained after centrifugation at 7000 rpm for 5 min was resuspended in 100 µL of sterile distilled water. The samples were heated at 100 °C for 10 min in a dry block heater, followed by centrifugation at 10,000 rpm for 10 min. The supernatant containing the template DNA was transferred to fresh tubes and stored at –20 °C until amplification [37].

Table 1 Specific Primer Sequences for the blaTEM Beta-lactamase Gene

Gene Name	Primer Name	Primer Sequence (5′→3′)
TEM	Forward (F)	ATG AGT ATT CAA CAT TTC CG
	Reverse (R)	CCA ATG CTT AAT CAG TGA GG

The PCR reaction mixture (25 µL final volume) consisted of 1 µL of each primer (10 pmol/µL), 0.5 µL of template DNA, 12.5 µL of 2× Taq PCR Master Mix (GENALL, South Korea), and 10.0 µL of PCR-grade water. Amplification was performed in a thermal cycler under the following conditions: initial denaturation at 94 °C for 10 min; 30 cycles of denaturation at 94 °C for 1 min, annealing at 55.5 °C for 1 min, and extension at 72 °C for 45 s; followed by a final extension at 72 °C for 5 min. The PCR products were resolved on a 1% agarose gel stained with ethidium bromide (0.5 µg/mL) in 1× TAE buffer and visualized using a gel documentation system under UV transillumination. A 1000 bp DNA ladder was used as a molecular size marker. *E. coli* ATCC 25923 was used as a quality control strain.

Antimicrobial Activity of AgNPs against *E. coli* Carrying the *TEM* Gene

The antibacterial efficacy of the biosynthesized AgNPs against *TEM*-positive *E. coli* isolates was evaluated using the agar disk diffusion method. Briefly, Mueller-Hinton Agar plates were inoculated with a bacterial suspension adjusted to 0.5 McFarland standard. Sterile paper disks (6 mm diameter, Padtan Teb Co.) were impregnated with 20 µL of different AgNP concentrations (5, 10, 15, 20, 25, 30, 35, and 40 µg/mL). Disks loaded with sterile distilled water served as negative controls, while disks containing tetracycline (30 µg) served as positive controls. The plates were incubated at 37 °C for 24 h. Afterward, the zone of inhibition (ZOI) around each disk was measured using a digital caliper. To ensure statistical reliability, all assays were performed with three independent biological replicates, each consisting of three technical replicates (N=9 observations per treatment).

Determination of MIC and Minimum Bactericidal Concentration (MBC)

The Minimum Inhibitory Concentration (MIC) and Minimum Bactericidal Concentration (MBC) were determined using the broth microdilution method in 96-well microtiter plates according to CLSI guidelines. The concentrations of AgNPs ranged from 0.5 to 128 µg/mL through two-fold serial dilutions in Mueller-Hinton Broth according to Table 2. Each well was inoculated with 10µL of the bacterial suspension to achieve a final concentration of approximately 5×10^5 CFU/mL. Wells with MHB and bacteria without AgNPs served as positive growth controls, while wells containing only MHB and AgNPs served as sterility controls. The plates were incubated at 37 °C for 24 h. The MIC was defined as the lowest concentration of AgNPs that completely inhibited visible bacterial growth (turbidity).

To determine the MBC, 10 µL of suspension from all wells showing no visible growth was plated onto fresh Mueller-Hinton Agar and incubated at 37 °C for 24 h. The MBC was recorded as the lowest concentration that reduced the viability of the initial bacterial inoculum by ≥99.9%. These assays were performed in triplicate (three independent biological replicates and three technical replicates).

Table 2 Titration Scheme of *N. oleander* Aqueous Extract for MIC Determination

	Tube 1	Tube 2	Tube 3	Tube 4	Tube 5	Tube 6	Tube 7	Tube 8
Mueller-Hinton Broth (mL)	0.1	0.1	0.1	0.1	0.1	0.1	0.1	0.1
Silver Nanoparticles (mL)	0.1	0.1	0.1	0.1	0.1	0.1	0.1	-
Sterile Distilled Water (mL)	-	-	-	-	-	-	-	0.1
Microbial Suspension (mL)	0.1	0.1	0.1	0.1	0.1	0.1	0.1	0.1
Final Concentration (Âµg/mL)	128	64	32	16	8	4	2	0

Effect of AgNPs on b*laTEM* Gene Expression

To investigate the sub-inhibitory effect of the biosynthesized AgNPs on the transcription of the *blaTEM* gene, six representative *E. coli* isolates harboring the gene were exposed to sub-MIC levels (16 µg/mL, equivalent to 1/2 MIC) of AgNPs. Briefly, the isolates were cultured in peptone broth at 37 °C in the presence and absence of AgNPs for 24 h [38]. Total RNA was extracted from treated and untreated cultures using the Pars Tous Biotech RNA extraction kit (Cat No. 5292, Iran) according to the manufacturer's instructions. The concentration and purity of the extracted RNA were verified using a NanoDrop spectrophotometer (Thermo Scientific, USA), and RNA integrity was assessed by agarose gel electrophoresis. cDNA synthesis was performed using the Genet Bio cDNA Synthesis Kit (Cat. No: Q9210, South Korea) starting from 1 µg of template RNA.

Quantitative Real-Time PCR (qPCR) was conducted in an Applied Biosystems StepOnePlus system. The reaction mixture (20 µL) consisted of 10 µL of 2× Prime QMaster Mix (with SYBR Green, Genet Bio), 1 µL of each primer (10 pmol), 1 µL of ROX reference dye, 2 µL of cDNA template, and 6 µL of nuclease-free water. The amplification profile included: initial denaturation at 95 °C for 15 min;

followed by 40 cycles of 95 °C for 30 s, 58 °C for 30 s, and 72 °C for 30 s. The 16S rRNA gene was utilized as an internal housekeeping reference gene for normalization. Relative expression levels were calculated using the $^{2-}\Delta\Delta CT$ method (Pfaffl method). All qPCR assays were performed with three biological and three technical replicates. Researchers have identified melting curve analysis with Real Time PCR as a highly sensitive technique for quickly detecting this bacterium [39]. The technique works by monitoring DNA denaturation through temperature changes which lead to DNA melting and generate a typical sigmoidal melting curve [40].

Protein Structure Retrieval and Molecular Docking Protocol

The amino acid sequences of *blaTEM* from *Escherichia coli* (GenBank: KX462012.1) and oleander methyltransferase from *N. oleander* (GenBank: MH504111.1) (Fig. 2) were retrieved from the NCBI database. (https://www.ncbi.nlm.nih.gov/). UniProt (https://www.uniprot.org/) is considered one of the most comprehensive and reliable resources for protein information [41].

Homology modeling and three-dimensional (3D) structure predictions were performed using the SWISS-MODEL server and AlphaFold2 database. The structural coordinates were optimized, and energy minimization was performed using the Swiss-PdbViewer.

To explore the potential computational affinity and binding interaction between the *E. coli blaTEM* protein (receptor) and the plant-derived *N. oleander* methyltransferase protein (ligand), protein-protein docking was executed using the ClusPro 2.0 web server. ClusPro calculates the docking conformations based on three steps: rigid-body docking using the PIPER Fourier transform (FT) correlation approach, energy-minimization refinement using the CHARMM forcefield, and clustering of the lowest energy configurations. The final complexes were selected based on the largest cluster size and the lowest electrostatic and hydrophobic binding free energy (ΔGbind in kcal/mol). Visual representation and interaction analysis of the binding interface (hydrogen bonds, salt bridges, and hydrophobic interactions) were carried out using PyMOL (v2.5) and LigPlot.

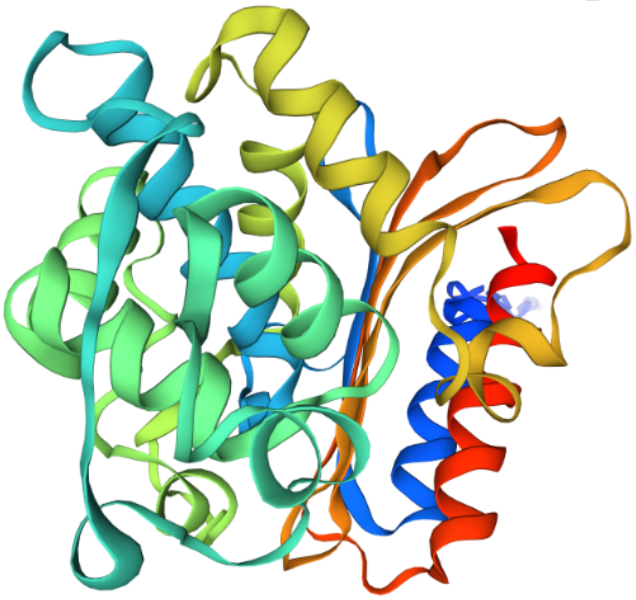

Fig. 1 3D structure of *blaTEM* protein (*Escherichia coli* (GenBank: KX462012.1))

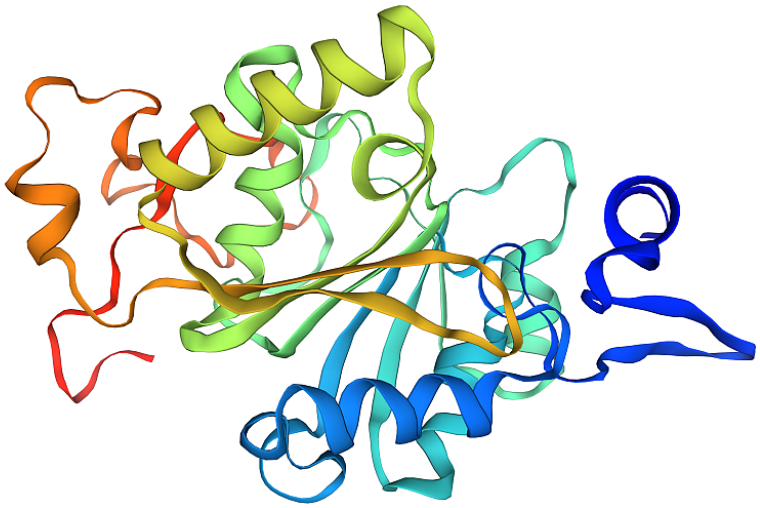

Fig. 2 3D structure of oleander methyltransferase protein (*N. oleander* (GenBank: MH504111.1))

Statistical Analysis

The experimental data were obtained from three independent experiments (N=3 biological replicates), each run-in triplicate (technical replicates). Data were analyzed using a completely randomized design (CRD). Statistical significance was determined using one-way

analysis of variance (ANOVA) followed by Duncan's multiple range test at a significance level of $p<0.05$ using SPSS software (v23.0). All graphical representations were generated using Microsoft Excel 2013 and GraphPad Prism 8.0.

RESULTS

Isolation and Identification of *E. coli* Strains Causing UTIs

Out of 155 urine samples collected from patients with clinical symptoms of urinary tract infections (UTIs) in Jiroft County, 155 *Escherichia coli* isolates were successfully recovered and identified. The taxonomic validation of these isolates was confirmed through morphological characterization and biochemical profiling. All isolates exhibited Gram-negative bacillary morphology and demonstrated typical biochemical behaviors of the Enterobacteriaceae family, as summarized in Table 3. While Figure 3 illustrates the IMViC test results. Scientists stored the confirmed isolates at –20 °C to use them in later experiments.

On Eosin Methylene Blue (EMB) agar, the isolates formed distinctive green metallic sheen colonies (Fig. 3A). The classical IMViC profile (++−−) confirmed the biochemical identity of the strains as *E. coli* (Fig. 3B).

Table 3 Biochemical and Physiological Profiles of *E. coli* Isolates Recovered from UTIs

Biochemical Tests	Result
Catalase	+
Triple sugar agar TSI	+
Indole production	+
Methyl red	+
Urease	-
Voges proskauer	-
Simmon's citrate	-
H2S	-

* Positive (+), Negative (-)

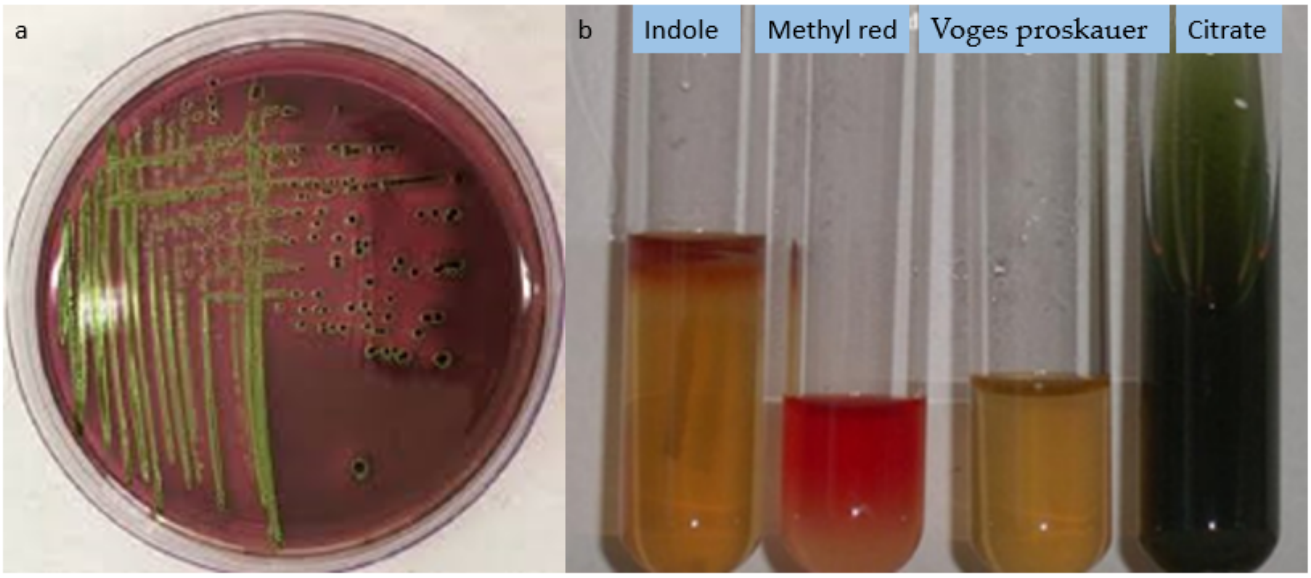

Fig. 3 Growth of *E. coli* on EMB medium showing metallic sheen (a) and IMViC biochemical test results (b)

Screening and Prevalence of ESBL-producing *E. coli*

Screening of the 155 confirmed *E. coli* isolates using the phenotypic double-disk synergy (DDS) test revealed a high prevalence of Extended-Spectrum *Beta-Lactamase* (*ESBL*) producers. Among the isolates, 100 strains (64.5%, reported as approximately 65%) were confirmed as ESBL-positive based on the CLSI criteria (Fig. 4). The synergistic enhancement of the inhibition zone between the ceftazidime/cefotaxime disks and their corresponding clavulanic acid-combined disks indicated the presence of class A beta-lactamases, which are inhibited by clavulanic acid.

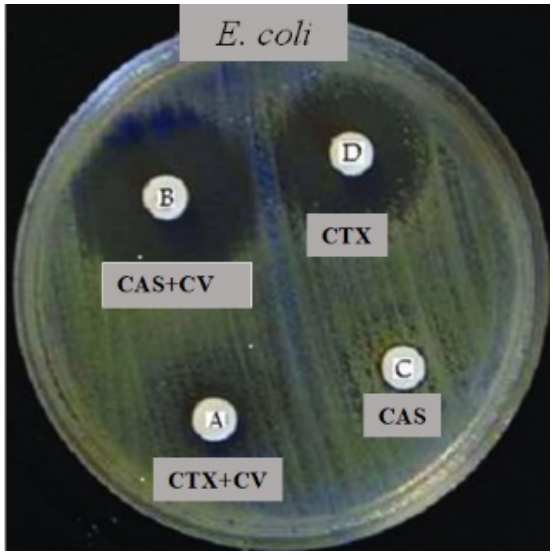

Fig. 4 Phenotypic confirmation of extended-spectrum *beta-lactamase* (ESBL) production in *Escherichia coli* isolates.

Antibiotic Susceptibility Profile of *E. coli* Isolates

The susceptibility patterns of the *E. coli* isolates against ten commonly prescribed antibiotics were evaluated using the Kirby-Bauer disk diffusion method. The quantitative zones of inhibition (ZOIs) are shown in Figures 5 and 6, and the overall resistance profile is depicted in Chart 1. The isolates exhibited high resistance to several traditional antimicrobial agents. High resistance rates were observed against ampicillin (10 µg, 74%), carbenicillin (100 µg, 61%), and chloramphenicol (30 µg, 53%). Data represent the mean values obtained from three independent biological replicates. Conversely, moderate to high sensitivity was recorded for aminoglycosides and fluoroquinolones, indicating their potential utility in non-*ESBL* cases, although the overall dissemination of multi-drug resistant (MDR) phenotypes remains a serious concern.

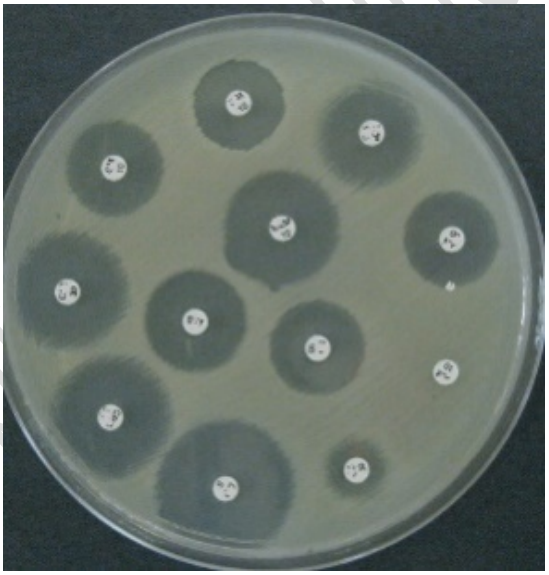

Fig. 5 Antibiotic susceptibility testing (AST) of uropathogenic *Escherichia coli* (UPEC) isolates using the Kirby-Bauer disk diffusion method.

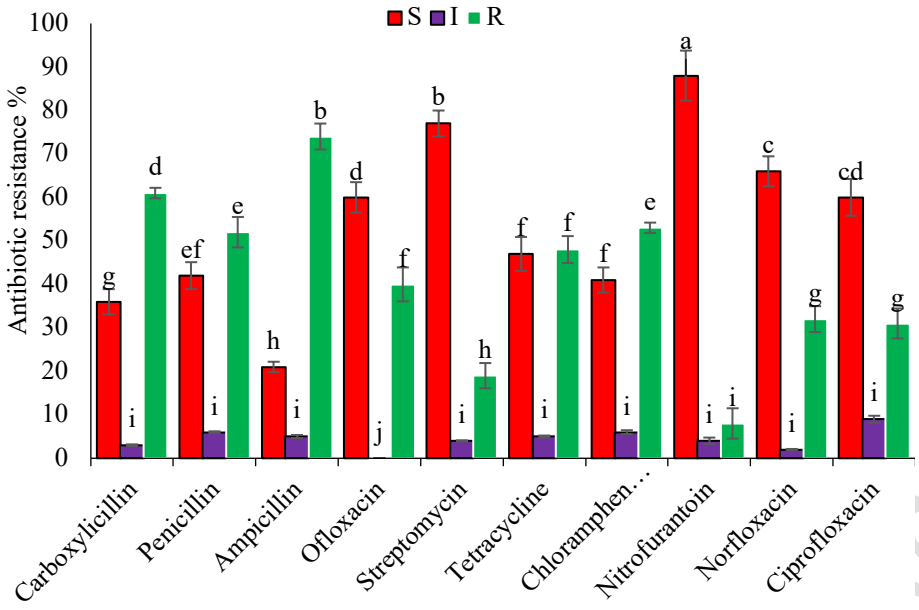

Fig. 6 Antibiotic susceptibility Profile of the *E. Coli* clinical Isolates based on inhibition zone diameter Resistant (R), Intermediate (I), and Susceptible (S).

Biosynthesis and Characterization of AgNPs

The green synthesis of silver nanoparticles (AgNPs) was achieved using the aqueous leaf extract of *N. oleander* (Fig. 7A, B). The photographic image illustrates the color transition of the reaction mixture (Aqueous extract + 1mM AgNO3) from light yellow to dark brown) (Fig. 8). This chromatic shift, observed within 2 h and intensified after 24 h of incubation at room temperature, indicates the reduction of silver ions (Ag+) to metallic silver nanoparticles (Ag0). This rapid color transition is attributed to the excitation of surface plasmon resonance (SPR) in the formed metal nanoparticles.

UV-Vis spectrophotometric analysis (Fig. 9) showed a prominent, symmetric SPR peak centered at 450 nm for the colloidal AgNP solution, whereas no absorption peak was detected for the raw *N. oleander* leaf extract which aligns with findings from Haji Rastamloo *et al*. [42]. The presence of a single peak in this range confirms the reduction of Ag^{+} to metallic silver (Ag^{0}) and indicates a relatively narrow size distribution of the nanoparticles.

Fig. 7 a) Representative photograph of *Nerium oleander* L. leaves collected from the Kerman province (Jiroft and Anbarabad regions) used for the biosynthesis of silver nanoparticles (AgNPs), b) Preparation of the aqueous leaf extract via the maceration method.

Fig. 8 Visual confirmation of the green synthesis of silver nanoparticles (AgNPs).

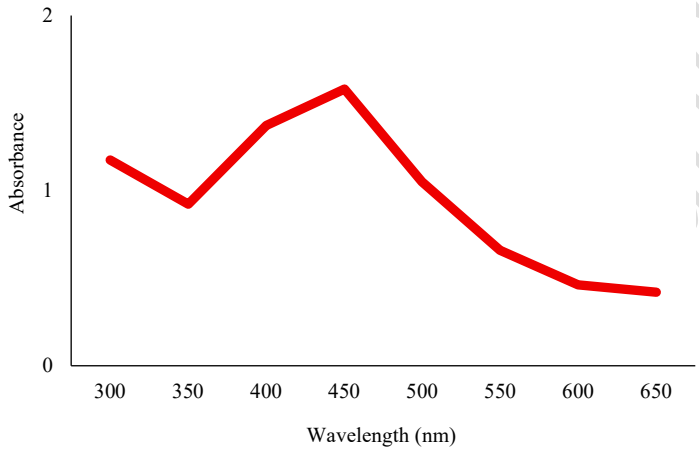

Fig. 9 UV-visible absorption spectra of the AgNPs synthesized with aqueous extract of *N. oleander*.

Detection of the *blaTEM* Gene via PCR

Molecular screening of the ESBL-positive isolates was performed using multiplex PCR targeting the *blaTEM* gene. Agarose gel electrophoresis revealed a specific band corresponding to the expected size of the *blaTEM* amplicon at approximately 850 bp (Figure 10). Out of 10 representative ESBL-producing isolates subjected to PCR validation, 6 (60%) harbored the *blaTEM* gene, demonstrating that the TEM-type enzyme is a key mediator of beta-lactam resistance in these clinical urinary isolates.

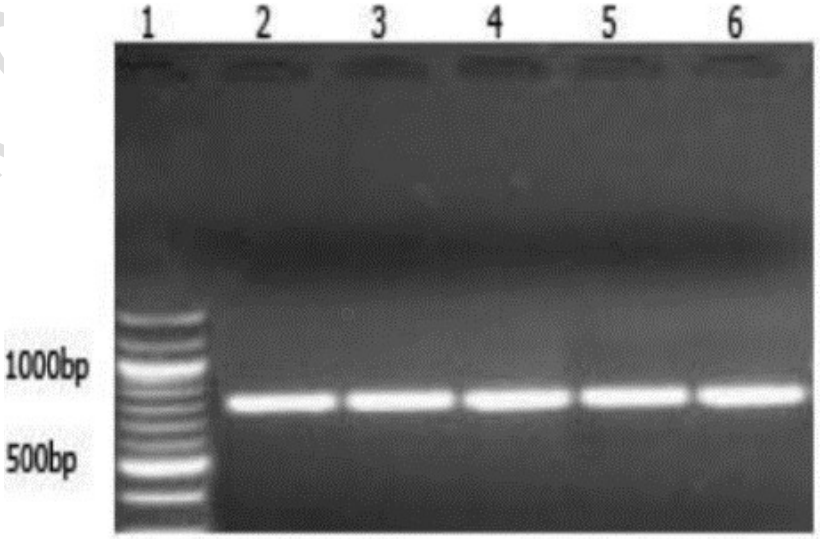

Fig. 10 Agarose gel electrophoresis (1.5% w/v) showing PCR amplification products of the *blaTEM* gene in *Escherichia coli* isolates. Lane 1: DNA ladder; Line 2: Positive control; Lanes 3–6: Amplified *blaTEM* gene products (size: 850 bp)

Antibacterial Efficacy of Green-Synthesized AgNPs against *E. coli* carrying the *TEM* Gene

The antibacterial activity of the biosynthesized AgNPs against the *blaTEM*-positive *E. coli* strains was assessed quantitatively. The disk diffusion assay showed that the AgNPs produced concentration-dependent zones of inhibition (Fig. 11).

The mean diameters of the inhibition zones ranged from 9.2 ± 0.4 mm at a concentration of 10 µg/mL to 22.5 ± 0.8 mm at 40 µg/mL ($p<0.05$). The positive control (tetracycline, 30 µg/mL) produced an inhibition zone of 18.4 ± 0.5 mm. These results demonstrate that the biosynthesized AgNPs possess significant antibacterial potency against drug-resistant clinical isolates. And this suggests a strong correlation between nanoparticle concentration and the disruption of bacterial growth. The bar chart represents the mean diameters of inhibition zones (mm) obtained via the agar well diffusion method at varying concentrations (10, 20, 30, and 40 µg/mL). A clear concentration-dependent increase in the zone of inhibition is observed, with maximum activity at 40 µg/mL. Results are presented as mean ± SD from three independent biological replicates ($p<0.05$).

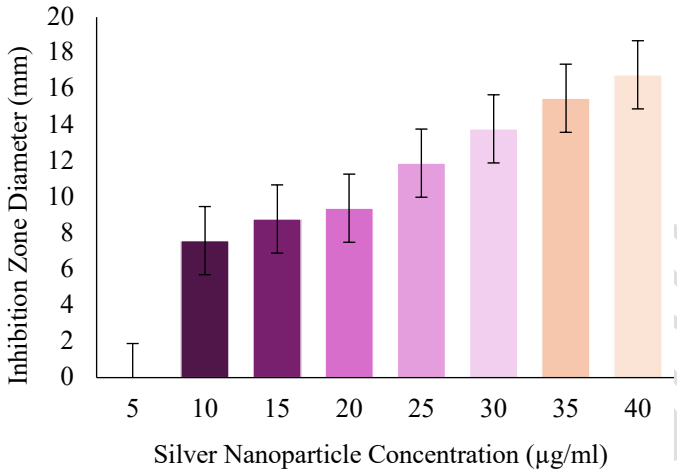

Fig. 11 Comparative dose-response analysis of phyto-synthesized silver nanoparticles against clinical ESBL-producing *E. coli* isolates carrying the *blaTEM* resistance determinant.

Determination of MIC and MBC

The microdilution assay was used to determine the Minimum Inhibitory Concentration (MIC) and Minimum Bactericidal Concentration (MBC) of the AgNPs (Tables 4 and 5). Values are expressed in µg/mL. The MIC was determined as the lowest concentration with no visible turbidity, while MBC was the lowest concentration resulting in zero colony growth on agar plates.The MIC of the biosynthesized AgNPs was determined to be 16 µg/mL (Table 4), indicating the lowest concentration capable of preventing visible bacterial replication.

Table 4 Minimum Inhibitory Concentration (MIC) of *N. oleander*-derived AgNPs against ESBL-producing *E. coli*

Type of Extract	2 µg/mL	4 µg/mL	8 µg/mL	16 µg/mL	32 µg/mL	64 µg/mL	128 µg/mL	Control
N. oleander	+	+	+	-	-	-	-	+

* Visible turbidity / bacterial growth (+), No visible turbidity / inhibition of growth (-).

Table 5 Minimum Bactericidal Concentration (MBC) of *N. oleander*-derived AgNPs against ESBL-producing *E. coli*

Type of Extract	2 µg/mL	42 µg/mL	82 µg/mL	162 µg/mL	322 µg/mL	642 µg/mL	1282 µg/mL	Control
N. oleander	*	*	*	*	+	+	+	–

*: Not tested (due to growth in MIC phase), +: Complete bactericidal effect (no colonies), –: Bacterial growth

The MBC was established at 32 µg/mL(Table 5), which is twice the MIC value. This low MBC/MIC ratio (≤2) demonstrates that the green-synthesized AgNPs act primarily through a bactericidal mechanism rather than a bacteriostatic one against these clinical isolates. Multiple researchers have documented the wide-ranging antibacterial properties of silver nanoparticles that work against antibiotic-resistant bacteria [38].

Effect of AgNPs on the Expression of the *blaTEM* Gene

Quantitative Real-Time PCR was performed to evaluate changes in transcription levels of the *blaTEM* resistance gene in six representative *E. coli* isolates after exposure to a sub-inhibitory concentration of AgNPs (16 µg/mL). Exposure to AgNPs significantly reduced the expression of the *blaTEM* gene (Table 6, Figures 12, 13, and 14). The mean relative expression level of the *blaTEM* gene in treated isolates dropped to 49±0.03 compared to the untreated control group (normalized to 1.0), representing a 48.5% reduction in mRNA levels ($p<0.05$). The housekeeping gene (16S rRNA) showed stable expression before and after treatment (ΔCT=0.45), confirming its validity as an internal reference. Melting curve analysis (Figure 15) showed single, sharp, and symmetric peaks with no secondary peaks or primer-dimer signals, confirming the specificity of the qPCR amplification.

Table 6 Relative Ct Values and *blaTEM* Expression Levels in *E. coli* Exposed to Biosynthesized AgNPs

$^{2-}$ ΔΔCT Control sample	$^{2-}$ ΔΔCT Oleander-treated sample	ΔΔCT Oleander-treated sample	ΔCT Control sample	ΔCT Oleander-treated sample
1	0.53	0.9	8.85	9.75

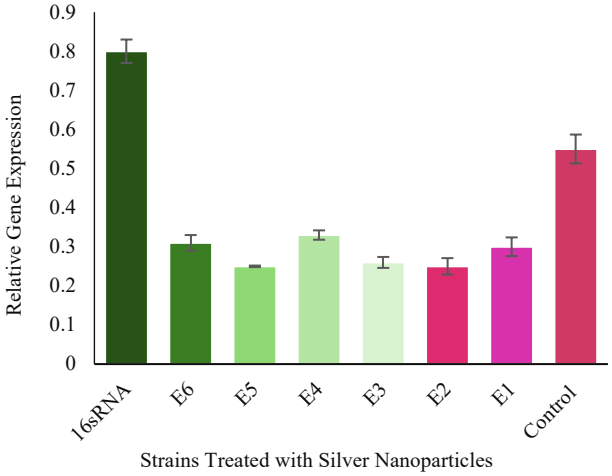

Fig. 12 Relative expression levels of the *blaTEM* gene in six representative *E. coli* isolates treated with biosynthesized AgNPs (16 µg/mL).

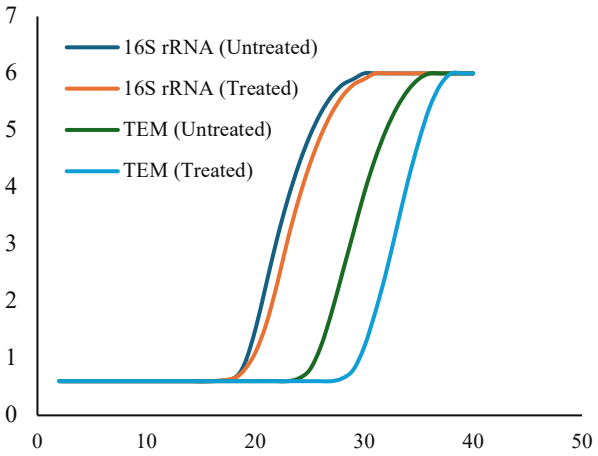

Fig. 13 Amplification curves for the *blaTEM* Gene before and after treatment with AgNPs, and amplification progress of the 16S rRNA housekeeping gene with calculated Ct values

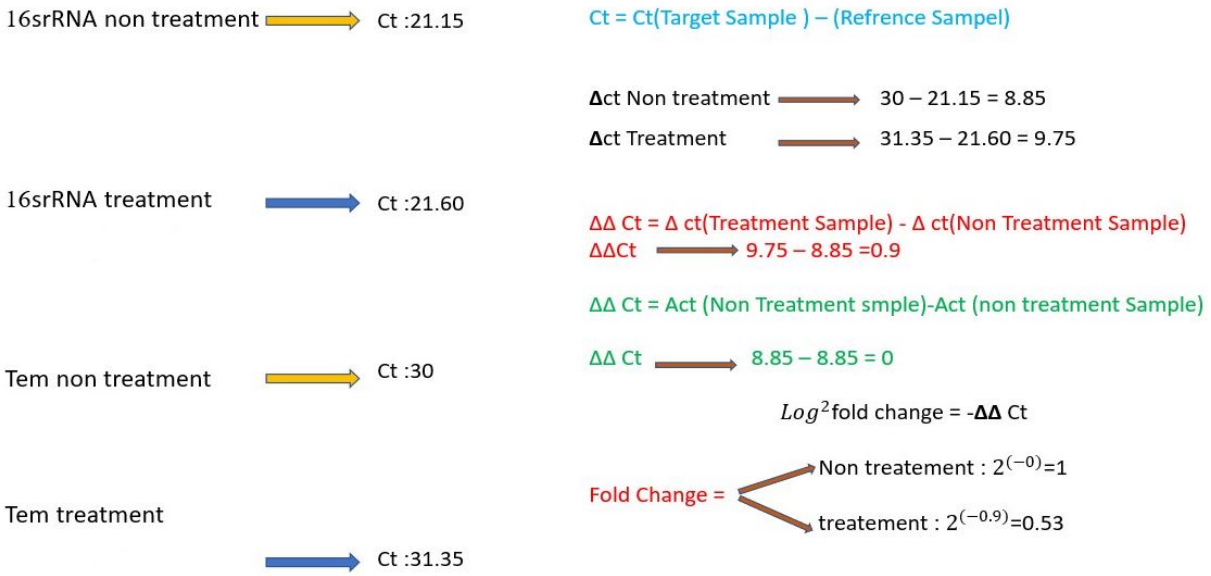

Fig. 14 Real-Time PCR results showing the effect of biosynthesized silver nanoparticles from *N. oleander* extract on *blaTEM* Gene expression in *E. coli*

Relative quantification of *blaTEM* mRNA was performed using the Pfaffl method, assuming 100% amplification efficiency for both the target and the 16S rRNA reference gene.

Expression analysis was performed using the $^{2-}$ΔΔCt formula. Table 6 demonstrates that silver nanoparticles produced from *N. oleander* decreased *blaTEM* gene expression but did not alter 16S rRNA expression. Researchers performed melting curve and amplification plot analyses to better understand how silver nanoparticles quantitatively affect *blaTEM* gene expression post-cDNA synthesis.

The presence of a single, sharp peak confirms the specificity of the PCR products and the absence of primer-dimers or non-specific amplification, ensuring the reliability of the quantitative expression data.

Homology Modeling and Structural Validation of Target and Ligand Proteins

To perform in silico protein-protein docking, three-dimensional (3D) structures of the target and ligand proteins were generated and validated.

For the target *blaTEM* protein (*E. coli*, GenBank: KX462012.1), the Ramachandran plot analysis showed that 94.01% of the residues were located in the most favored regions, indicating a highly reliable stereochemical conformation (Fig. 15). The global quality of the model was further validated by a high QMEANDisCo score of 89±0.05, indicating structural alignment with experimentally resolved templates (Fig. 16). The normalized QMEAN4 Z-score (Fig. 17) fell within the typical range ($|Z|<1$), confirming that the template selection and structural optimization were appropriate.

For the ligand, *N. oleander* methyltransferase (GenBank: MH504111.1), structural validation using the Ramachandran plot (Fig. 18) showed that 95.92% of the residues fell within the favored energy regions. The QMEANDisCo local quality analysis (Figure 19) and the global QMEAN Z-score (Fig. 20) showed a value of 0.59 ± 0.05, confirming that the generated model is structurally plausible and suitable for computational molecular docking.

The Ramachandran Favoured percentage of 94.01% indicates that the vast majority of residues in the protein structure adopt energetically favorable phi (φ) and psi (ψ) dihedral angles, suggesting a high-quality model with minimal steric clashes. This figure lists a series of angles (e.g., 180°, 0°, -180°), likely representing φ/ψ pairs for individual residues, which—though not visualized as a traditional 2D Ramachandran plot—hint at conformations typical of β-strands (ψ ≈ ±180°) or α-helices (φ ≈ -60°, ψ ≈ -45°). The repeated -180° values may reflect extended β-sheet regions, while the 6% non-favoured residues could arise from flexible loops or functional sites. For precise interpretation, plotting these angles on a Ramachandran diagram (e.g., using PyMOL or RAMPAGE) would clarify their distribution and highlight any outliers requiring further validation (Fig. 15).

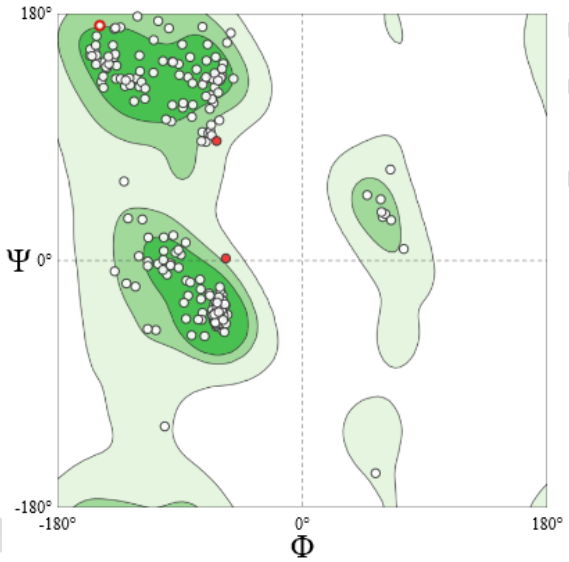

Fig. 15 Ramachandran chart for the 3D structure of *blaTEM* protein (*Escherichia coli* (GenBank: KX462012.1))

The Local Quality Estimate - All Chains figure, combined with the QMEANDisCo Global score of 0.89 ± 0.05, provides a comprehensive assessment of the protein model's reliability. The local similarity scores, ranging from 0.3 to 240, indicate regions of varying confidence, with higher values (e.g., ≥150) corresponding to well-resolved structural elements and lower values (e.g., ≤30) potentially highlighting less reliable segments. The high QMEANDisCo Global score (0.89±0.05, where scores closer to 1 indicate better agreement with experimental structures) further supports the overall quality of the model, suggesting that the global fold is accurately predicted. However, discrepancies in local similarity scores emphasize the need for targeted refinement of specific regions, particularly those with low predicted similarity, to ensure uniformity in model accuracy. Together, these metrics underscore a generally robust structure while pinpointing areas for further optimization (Fig. 16).

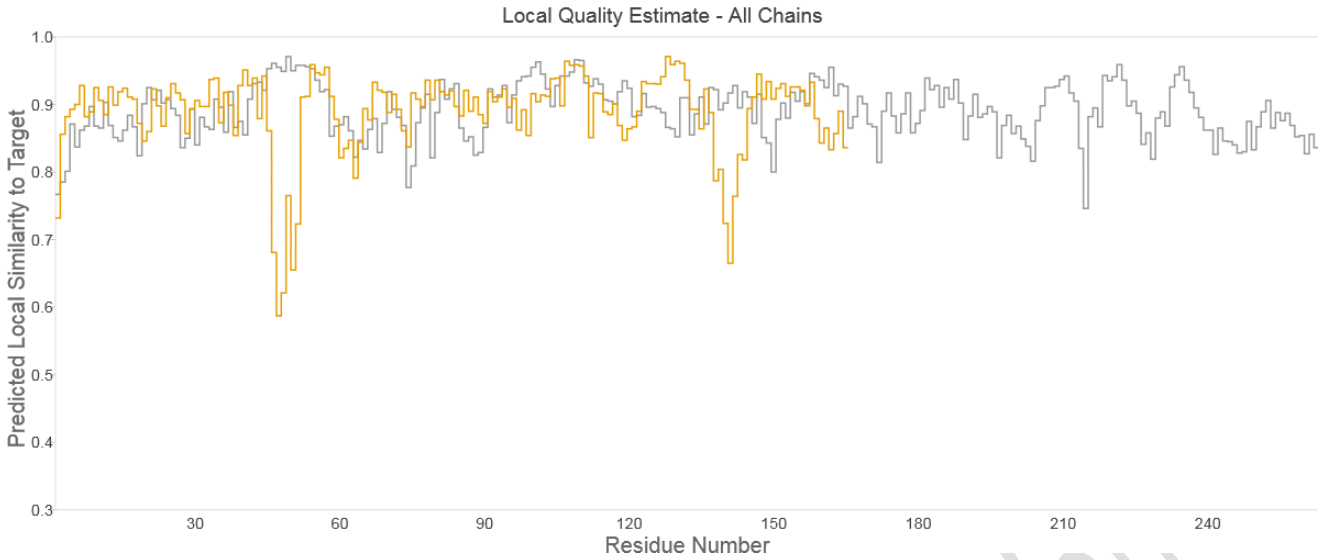

Fig. 16 The QMEANDisCo Local for the 3D structure of *blaTEM* protein (*Escherichia coli* (GenBank: KX462012.1))

The Normalized QMEAN4 Score provides a statistical assessment of the model's quality relative to experimentally determined structures in the PDB. The Z-score categorization reveals how the model performs against a non-redundant set of PDB structures: scores within |Z−score|<1|Z−score|<1 indicate the model's quality is comparable to typical high-resolution structures, while |Z−score|>2|Z−score|>2 suggests significant deviations. The displayed fractions (e.g., 100200200100) likely represent the distribution of residues across these Z-score ranges, highlighting the proportion of the structure that meets or deviates from expected quality benchmarks. Combined with the QMEANDisCo Global score of 0.89 ± 0.05, this analysis confirms that the majority of the model adheres to high-quality standards, though targeted refinement may benefit residues falling outside the |Z−score|<1|Z−score|<1 range. This dual evaluation—global and local—ensures a balanced interpretation of the model's reliability for downstream applications (Fig. 17).

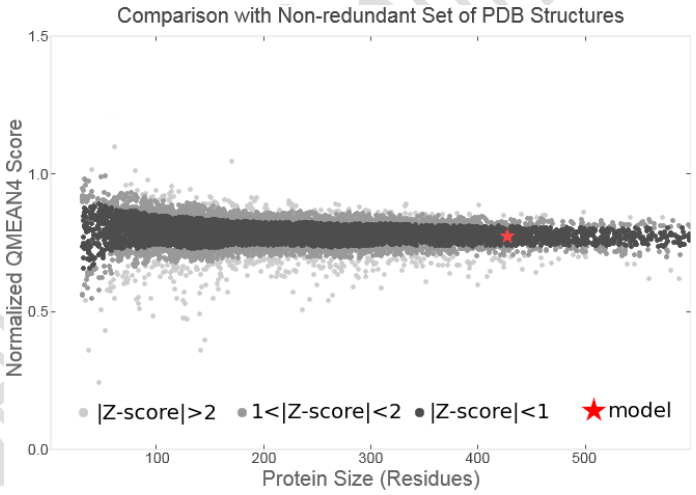

Fig. 17 Normalized QMEAN Z-Scores analysis for the 3D structure of *blaTEM* protein (*Escherichia coli* (GenBank: KX462012.1))

Ramachandran plot visualizes the distribution of the backbone dihedral angles (ϕϕ and ψψ) of amino acid residues in a protein structure. The plot highlights the energetically favored regions for these angles, which correspond to common secondary structures such as right-handed alpha helices and beta sheets. In the context of structure validation, the term "Ramachandran Favoured 95.92%" indicates that 95.92% of the residues in the analyzed protein fall within these favored regions, demonstrating excellent stereochemical quality and suggesting that the protein model is highly reliable. The dense clustering of points within the green-shaded favored areas in the figure visually confirms this high percentage, as most residues occupy the expected conformational space for well-folded proteins. This distribution is a strong indicator of correct protein folding and structural integrity, as a high percentage of residues in favored regions is a hallmark of high-quality protein structures (Figure 18).

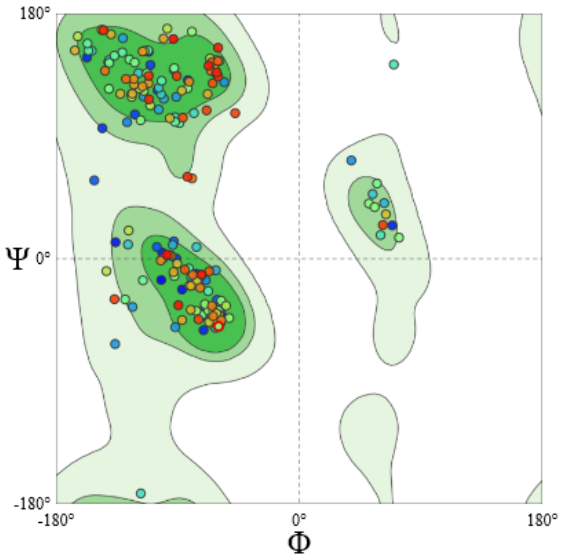

Fig. 1 Ramachandran plot analysis for the 3D structure of *N. oleander* methyltransferase (GenBank: MH504111.1)

The QMEANDisCo figure presents a local quality estimate for a protein structure, displaying the predicted local similarity to the target for each residue along the sequence. The y-axis quantifies the predicted local similarity, with higher values indicating regions of the model that closely resemble ideal or reference structures, while lower values highlight areas of potential structural uncertainty or deviation. The alternating purple and orange bars represent regions of higher and lower local quality, respectively, revealing a pattern of variable structural reliability throughout the protein. This variability is further summarized by the QMEANDisCo global score of 0.59 ± 0.05, which suggests that the overall model quality is moderate, with some regions exhibiting strong agreement with reference structures and others showing notable deviations. Such information is valuable for identifying well-modeled segments suitable for further analysis and regions that may require additional refinement or caution in interpretation (Fig. 19).

Fig. 19 QMEANDisCo Local for 3D structure of oleander methyltransferase protein (*N. oleander* (GenBank: MH504111.1))

Local quality estimate for the *N. oleander* methyltransferase model (Fig. 20). The plot shows a moderate global QMEANDisCo score of 0.59±0.05. The alternating bars highlight regions of high confidence (purple) and flexible loop regions (orange) that may require caution in docking interpretations.

The QMEAN Z-Scores figure illustrates the normalized QMEAN4 score of the protein model (marked by a red star) in comparison to a large, non-redundant set of experimentally determined protein structures from the Protein Data Bank (PDB). The x-axis represents protein size in terms of residue count, while the y-axis shows the normalized QMEAN4 score, a widely used indicator of protein model quality. Most reference structures cluster tightly around a normalized score near 1.0, with varying degrees of deviation indicated by different shades of gray based on their Z-scores. The position of the red star demonstrates that the model's normalized QMEAN4 score falls well within the typical range observed for experimentally validated structures of similar size, suggesting that the overall quality of the protein model is comparable to high-quality, experimentally solved proteins. This provides strong evidence for the reliability and structural plausibility of the model (Fig. 20).

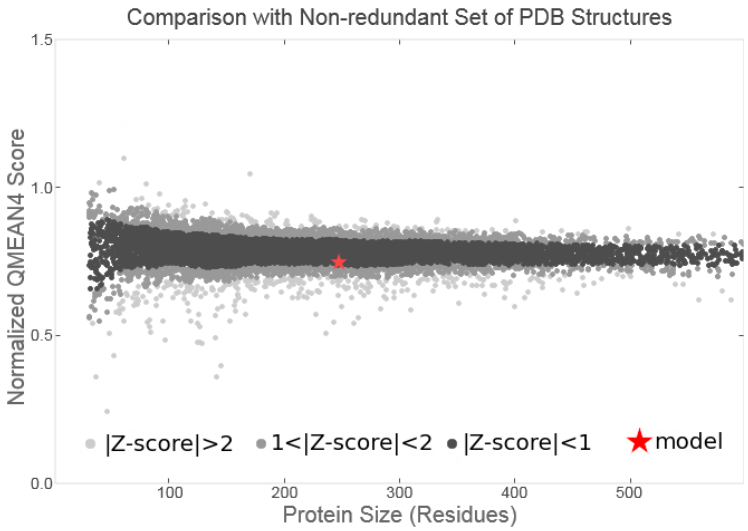

Fig. 20 QMEAN Z-Scores for 3D structure of oleander methyltransferase protein (*N. oleander* (GenBank: MH504111.1))

The molecular docking analysis between the ligand *oleander methyltransferase* and the target protein *blaTEM* demonstrated successful binding, with a stable complex formed primarily through hydrophobic interactions. Key hydrophobic amino acids—leucine (Leu), isoleucine (Ile), valine (Val), phenylalanine (Phe), and tryptophan (Trp)—played a crucial role in strengthening the binding affinity by forming a tightly packed nonpolar core at the interaction interface. These residues facilitated strong van der Waals forces and π-π stacking (particularly with Phe and Trp), enhancing the stability of the docked complex. Computational binding energy calculations and residue interaction analysis confirmed that these hydrophobic contacts were critical for the robust and specific binding observed in this docking study (Fig. 21A, B).

In protein-protein docking, tryptophan (Trp, W) is often considered the most critical amino acid for forming tight binding (Fig. 21A) due to its unique aromatic and hydrophobic properties. Its large indole ring facilitates strong π-π stacking, cation-π interactions, and van der Waals contacts at the protein-protein interface, enhancing binding affinity and specificity. Studies show that Trp frequently appears in hot spot regions of protein complexes, contributing significantly to stabilization. For instance, a study [39] highlights that tryptophan, along with other hydrophobic residues like tyrosine (Tyr) and arginine (Arg), is enriched at high-affinity interfaces, underscoring its pivotal role in secure molecular docking.

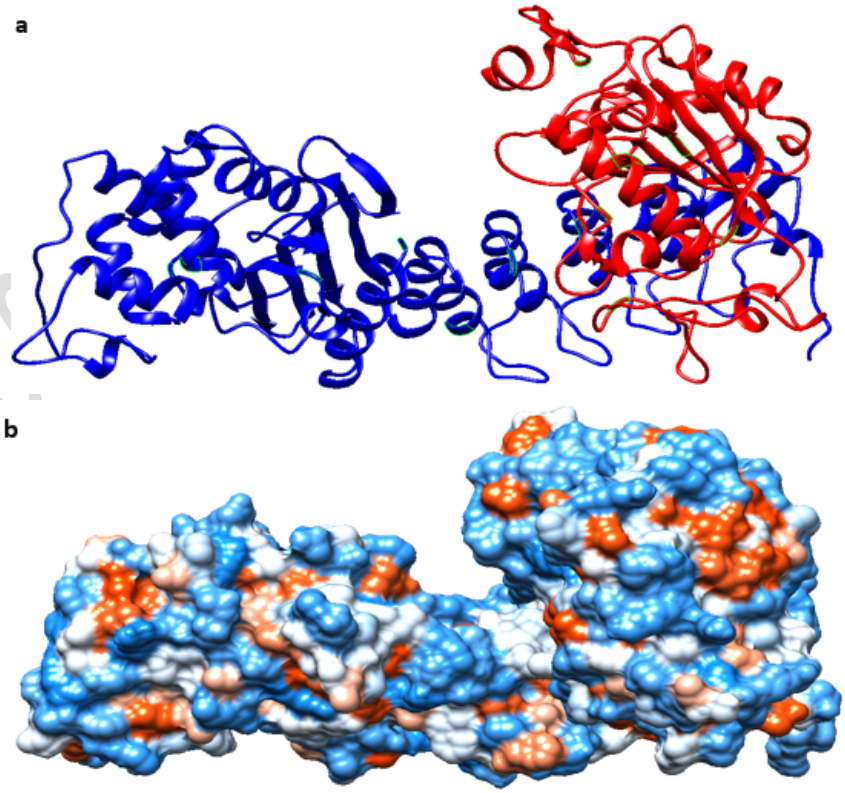

Fig. 21 a) The present of tryptophan and b) docking between ligand (*oleander methyltransferase*) and target (*blaTEM*) protein

DISCUSSION

Urinary tract infections (UTIs) remain one of the most common bacterial infections worldwide, and *Escherichia coli* is recognized as the leading causative agent in the majority of cases. In the present study, the high recovery rate of *E. coli* from urine samples confirms its

dominant role in UTIs in the studied region and is consistent with previous reports describing this organism as the principal uropathogen [45]. More importantly, the emergence of multidrug-resistant strains has made the clinical management of these infections increasingly difficult, contributing to therapeutic failure, prolonged hospitalization, and increased mortality [46].

A major driver of resistance in *E. coli* is the production of beta-lactamases, particularly extended-spectrum beta-lactamases (ESBLs), which hydrolyze broad-spectrum cephalosporins and related beta-lactam antibiotics. ESBL-encoding genes are often located on transferable plasmids, enabling rapid dissemination among bacterial populations and contributing to geographic and temporal variation in resistance prevalence [47]. This mobility makes ESBL-producing strains especially problematic in healthcare settings, where they are associated with limited treatment options and higher clinical risk [48]. The prevalence of ESBL-producing *E. coli* observed in this study further supports the growing concern that beta-lactam resistance is becoming deeply established in clinical isolates from UTIs.

The prevalence of ESBL production in *E. coli* varies considerably between countries and even between regions within the same country. Previous studies in Iran have reported ESBL rates ranging from 33% to 68%, reflecting the ongoing spread of resistant strains in both community and hospital settings [49,50]. Soltan Dallal et al. also documented a marked rise in ESBL-producing isolates over time, from 15.62% to 64% between 2007 and 2011 [51]. Comparable trends have been reported elsewhere. For example, beta-lactamase-producing *E. coli* has been implicated in severe bloodstream infections with high mortality rates [52]. Collectively, these findings emphasize that ESBL-producing *E. coli* is no longer a localized issue but a broad public health challenge.

In the present work, 155 *E. coli* isolates were identified from UTI samples collected in Jiroft, and 100 isolates (65%) were confirmed as beta-lactamase producers by CLSI-based phenotypic testing. This prevalence is broadly consistent with several previous reports and indicates that resistant *E. coli* strains are highly represented in the local clinical population. PCR analysis further showed that 60% of the tested ESBL-positive isolates carried the *blaTEM* gene, suggesting that TEM-type beta-lactamase is one of the major resistance determinants in these isolates. This is in agreement with reports from Sweden, India, Turkey, and Iran, where *blaTEM* has been detected at variable but substantial frequencies among ESBL-producing *E. coli* isolates [53-55]. These data collectively indicate that *blaTEM* remains an important molecular marker of beta-lactam resistance in urinary isolates.The antibiotic susceptibility profile also demonstrated substantial resistance to commonly used drugs, with the highest resistance observed against ampicillin, followed by carbenicillin and chloramphenicol. These results are consistent with prior studies showing that indiscriminate antibiotic exposure has accelerated resistance in Enterobacteriaceae [56-60]. The elevated resistance to *beta-lactams* is particularly concerning because these drugs are frequently used as first-line or empiric therapies. Such resistance limits treatment options and underscores the need for continued surveillance and more judicious antibiotic prescribing. Given the limitations of conventional antibiotics, the search for alternative antimicrobial agents has intensified. Among these, silver nanoparticles (AgNPs) have attracted considerable attention because of their strong antimicrobial activity, small size, high surface-area-to-volume ratio, and potential for surface functionalization [61,62]. In addition, green synthesis approaches are increasingly preferred because they avoid harsh chemicals and can utilize plant-derived reducing and stabilizing agents. In this study, *Nerium oleander* extract successfully mediated the synthesis of AgNPs, as indicated by the color change from pale yellow to dark brown and the appearance of a characteristic surface plasmon resonance peak at 450 nm. This spectral shift is a hallmark of AgNP formation and reflects the collective oscillation of conduction electrons at the nanoparticle surface [34,63,64].

The antibacterial activity of the synthesized AgNPs against *E. coli* was concentration dependent, with larger inhibition zones observed as the nanoparticle concentration increased. The MIC and MBC values of 16 and 32 µg/mL, respectively, indicate that the biosynthesized AgNPs exert a bactericidal effect rather than merely inhibiting growth. These findings are in agreement with earlier studies showing that plant-mediated AgNPs can inhibit both Gram-negative and Gram-positive bacteria [65,66]. The observed antimicrobial effect may be explained by several complementary mechanisms, including disruption of the bacterial cell membrane, interaction with thiol-containing proteins, generation of reactive oxygen species, interference with respiration, and damage to DNA and intracellular proteins [67-75]. Because AgNPs can interact with multiple cellular targets simultaneously, bacteria are less likely to develop resistance against them as rapidly as they do against conventional single-target antibiotics.

A notable finding of this study was the significant reduction in *blaTEM* transcript levels after treatment with subinhibitory AgNP concentrations. Real-time PCR showed a 48.5% decrease in gene expression relative to untreated controls, which suggests that AgNP exposure may influence resistance-associated transcriptional activity. However, this result should be interpreted carefully. The present data demonstrate a transcriptional association, not direct gene deletion or permanent gene silencing. It is more appropriate to propose that AgNP-induced stress may alter bacterial physiology in ways that secondarily reduce *blaTEM* expression, possibly through membrane perturbation, oxidative stress, or disruption of regulatory pathways. Therefore, while the qPCR results are encouraging, they should be viewed as evidence of altered gene expression rather than definitive proof of direct genomic suppression.

The melting curve analysis confirmed the specificity of the qPCR products, with single sharp peaks indicating the absence of nonspecific amplification or primer-dimer formation. This supports the validity of the expression analysis and strengthens confidence in the observed reduction in *blaTEM* expression. Similar reductions in antibiotic resistance or virulence gene expression after AgNP exposure have been reported for other pathogenic bacteria, including methicillin-resistant Staphylococcus aureus and Acinetobacter baumannii [76-79]. These findings suggest that AgNPs may act not only as direct antimicrobial agents but also as modulators of bacterial stress responses and resistance-associated pathways.

The molecular docking analysis further suggested a favorable interaction between the modeled proteins, with a binding energy of -8.42 kcal/mol and stabilization contributed by hydrophobic residues, including tryptophan. Hydrophobic interactions and aromatic stacking are known to enhance complex stability in protein-protein interfaces, and the docking results therefore provide a plausible structural basis for the observed computational interaction. However, this finding should be interpreted strictly as an in silico hypothesis-generating result. Docking does not demonstrate that such an interaction occurs in living bacteria, nor does it prove that AgNPs directly bind to or inhibit *TEM beta-lactamase in vivo*. Thus, the docking analysis should be considered supportive but not conclusive. Future biochemical studies, enzymatic inhibition assays, and binding validation experiments will be required to determine whether the observed computational interaction has real functional significance.

Overall, the present study indicates that green-synthesized AgNPs derived from *N. oleander* possess promising antibacterial activity against ESBL-producing *E. coli* isolated from UTIs. Their efficacy appears to involve both direct bactericidal effects and a measurable reduction in *blaTEM* expression under subinhibitory exposure. Nevertheless, the molecular mechanism underlying this transcriptional change remains to be clarified. Additional work is needed to evaluate nanoparticle toxicity, pharmacological safety, stability, and in vivo efficacy before clinical application can be considered. Despite these limitations, the present findings support the potential of plant-mediated AgNPs as a promising adjunct or alternative strategy for combating antibiotic-resistant uropathogens.

CONCLUSION

In conclusion, this study demonstrated that silver nanoparticles (AgNPs) biosynthesized using *Nerium oleander* leaf extract possess significant antibacterial activity against ESBL-producing *E. coli* isolates under laboratory conditions. The results showed that these green-synthesized nanoparticles not only inhibit bacterial growth but also reduce the expression levels of the *blaTEM* resistance gene. While these findings are promising at the *in vitro* level, it is important to emphasize that this study did not include *in vivo* experiments, toxicity assessments, or clinical trials. Therefore, the potential for using these AgNPs as therapeutic agents or antibiotic alternatives remains speculative at this stage. The molecular docking results provide a theoretical framework for future interaction studies but do not constitute biological proof of efficacy in a clinical setting. Future research is strictly required to evaluate the biocompatibility, long-term stability, and safety of these nanoparticles in animal models and human cell lines. Until such comprehensive toxicological and pharmacological profiles are established, the biosynthesized AgNPs should be viewed as a subject for further laboratory exploration rather than a candidate for immediate clinical application.

Conflict of Interests

All authors declare no conflict of interest.

Ethics Approval and Consent to Participate

No human or animals were used in the present research.

Ethical Issues

Ethical issues (including plagiarism, data fabrication, double publication) have been completely observed by the authors. The authors have adhered to ethical standards, including avoiding plagiarism, data fabrication, and double publication.

Consent for Publication

All authors read and approved the final manuscript for publication.

Availability of Data and Material

All the data are embedded in the manuscript. The datasets generated and/or analyzed during this study are available from the corresponding author upon reasonable request.

Authors' contributions

Conceptualization: Z. F.
Data curation: N. H.
Formal analysis: M. Sh.
Investigation: A. S-S.
Methodology: B. F-N.
Project administration: A. S-S.
Resources: All authors.
Supervision: B. F-N.
Validation: Z. F., H. B.
Visualization: R. Gh.
Writing–original draft: Z. F.
Writing–reviewing & editing
All authors.

Informed Consent

The authors declare not used any patients in this research.

Funding

This research did not receive any specific grant from funding agencies in the public, commercial, or not-for-profit sectors.

Acknowledgement

This article was achieved based on the material and equipment of Research Institute of Zabol, that the authors thanks it.

REFERENCES

1. Soltan Dallal M.M., Rajabi Z., Papizadeh M., Amiri S., Foroushani A.R., Naser A., Mirbagheri S.Z., Masoumi-Asl H., Torabi P., Mirza Babaei M. Prevalence of extended-spectrum β-lactamase (ESBL)-producing Escherichia coli associated with outbreaks of food-borne gastroenteritis in Tehran. Cellular and Molecular Biomedical Reports. 2024;4(4):199-207.
2. Tula M.Y., Filgona J., Kyauta S.E., Elisha R. Screening for some virulence factors among bacterial isolates from surfaces of hospital fomites and hands of healthcare workers. Cellular and Molecular Biomedical Reports. 2023;3(1):9-16.

3. Bhattacharjee A., Sen M.R., Prakash P., Gaur A., Anupurba S. Increased prevalence of extended spectrum β-lactamase producers in neonatal septicaemic cases at a tertiary referral hospital. Indian Journal of Medical Microbiology. 2008;26(4):356-360.
4. Knothe H., Shah P., Krcmery V., Antal M., Mitsuhashi S. Transferable resistance to cefotaxime, cefoxitin, cefamandole and cefuroxime in clinical isolates of Klebsiella pneumoniae and Serratia marcescens. Infection. 1983;11(6):315-317.
5. Jacoby G.A., Medeiros A.A. More extended-spectrum beta-lactamases. Antimicrobial Agents and Chemotherapy. 1991;35(9):1697-1704.
6. Ambler R.P. The structure of β-lactamases. Philosophical Transactions of the Royal Society of London. B, Biological Sciences. 1980;289(1036):321-331.
7. Bonnet R. Growing group of extended-spectrum β-lactamases: the CTX-M enzymes. Antimicrobial Agents and Chemotherapy. 2004;48(1):1-14.
8. Calbo E., Romaní V., Xercavins M., Gómez L., Vidal C.G., Quintana S., Vila J., Garau J. Risk factors for community-onset urinary tract infections due to Escherichia coli harbouring extended-spectrum β-lactamases. Journal of Antimicrobial Chemotherapy. 2006;57(4):780-783.
9. M.S., M.N., M.S. Extended-spectrum beta-lactamase resistance in clinical isolates of Klebsiella pneumoniae and Escherichia coli in in-patient and out-patient groups. Medical Journal of Tabriz University of Medical Sciences. 2008;30(2):79-86.
10. Hamadamin H.Z., Shallal A.F., Qader I.N. Synergistic role of extended-spectrum beta-lactamases (ESBL) and bacterial structure on antibacterial drugs. Jabirian Journal of Biointerface Research in Pharmaceutics and Applied Chemistry. 2024;1(3):26-36.
11. Sinha M., Srinivasa H., Macaden R. Antibiotic resistance profile & extended spectrum beta-lactamase (ESBL) production in Acinetobacter species. Indian Journal of Medical Research. 2007;126(1):63-67.
12. Burcu B., Açik L., Sultan L. Phenotypic and molecular characterization of SHV, TEM, CTX-M and extended spectrum ß-lactamase produced by Escherichia coli, Acinetobacter baumannii and Klebsiella isolates in a Turkish hospital. African Journal of Microbiology Research. 2010;4:650-654.
13. Geyer C.N., Hanson N.D. Rapid PCR amplification protocols decrease the turn-around time for detection of antibiotic resistance genes in Gram-negative pathogens. Diagnostic Microbiology and Infectious Disease. 2013;77(2):113-117.
14. Hosseini-Mazinani S.M., Eftekhar F., Milani M., Ghandili S. Characterization of β-lactamases from urinary isolates of Escherichia coli in Tehran. Iranian Biomedical Journal. 2007;11(2):95-99.
15. Masjedian G., Valehi F., Talebi R.L.A., Rastegar L. Molecular evaluation of resistance to expanded antibiotics in Escherichia coli and Klebsiella pneumoniae. Iranian Journal of Medical Microbiology. 2007;1(2):27-34.
16. Allafchian A.R., Jalali S.A.H., Aghaei F., Farhang H.R. Green synthesis of silver nanoparticles using Glaucium corniculatum (L.) Curtis extract and evaluation of its antibacterial activity. IET Nanobiotechnology. 2018;12(5):574-578.
17. Reddy N.J., Nagoor Vali D., Rani M., Rani S.S. Evaluation of antioxidant, antibacterial and cytotoxic effects of green synthesized silver nanoparticles by Piper longum fruit. Materials Science and Engineering: C. 2014;34:115-122.
18. Marambio-Jones C., Hoek E.M.V. A review of the antibacterial effects of silver nanomaterials and potential implications for human health and the environment. Journal of Nanoparticle Research. 2010;12(5):1531-1551.
19. Naseriyeh T., et al. Can a nanoliposome be a suitable carrier for the local delivery of human growth hormone to achieve skin rejuvenation? Micro and Nano Bio Aspects. 2026;4(4):35-49.
20. Naseriyeh T., Abdi F., Ahmadifard Z., Kahrizi D. Nanoparticles reinforcing hydrogels: a novel approach to improving the properties of wound healing hydrogels. Advances in Applied Nano-Bio Technologies. 2025;6(1):8-23.
21. Ghorbani M., et al. Development and characterization of indole-3-butyric acid-functionalized Fe3O4@SiO2 nanoparticles for improved plant root development. BioNanoScience. 2025;15:329.
22. Ghorbani M., et al. Preparation and characterization of immobilized indole-3-butyric acid on silver-cerium oxide nanoparticles for improving its stability and utilization in the study of plant root formation indices. Frontiers in Plant Science. 2025;16:1570945.
23. Izadi M., et al. Nano-encapsulated ajwain essential oil elicits resistance against early blight in tomatoes. Cellular and Molecular Biology. 2025;71(5):1-5.
24. Fatemifard S.Z., Masoumiasl A., Fazeli-Nasab B., Piri R., Mirzaei A.R., Salehi Sardoei A., Ghorbanpour M. Exogenously applied silver nanoparticles (AgNPs) differentially affect bacterial blight disease control in twenty-seven wheat cultivars. BMC Plant Biology. 2024;24(1):695.
25. Javadian E., Biabangard A., Ghafari M., Saeeidi S., Fazeli-Nasab B. Green synthesis of silver nanoparticles and antibacterial properties of extracts of Capparis spinosa leaves. International Journal of Medicinal Plants and By-products. 2024;13(2):329-343.
26. Chahardooli M., Khodadadi E. The biosynthesis of silver nanoparticles using OAK fruit extract and the investigation of their anti-microbial activities against nosocomial infection agents. Journal of Ilam University of Medical Sciences. 2014;22:27-33.
27. Begum S., Sultana R., Siddiqui B.S. Triterpenoids from the leaves of Nerium oleander. Phytochemistry. 1997;44(2):329-332.
28. Wong S.K., Chan H.T., Chan E.W.C. Chemistry, resources, anticancer effects, other pharmacological properties, and clinical trials of oleandrin from Nerium oleander: an overview. Journal of Applied Pharmaceutical Science. 2025;15(12):004-012.
29. Zhai J., Dong X., Yan F., Guo H., Yang J. Oleandrin: a systematic review of its natural sources, structural properties, detection methods, pharmacokinetics and toxicology. Frontiers in Pharmacology. 2022;13:822726.
30. Bekhit A.A., Habib H.J., Hefnawy A., Nasralla S.N., Yusuf F.A., Al-Tamawi A.M., Al-Thawadi S.M., Bekhit S.A. Evaluation of the antibacterial activity of Nerium oleander leaves extract and its synergistic effect with ceftriaxone. Evaluation. 2024;47(10):8491-8501.
31. Saravani K., Ramezannezhad P., Malayeri F.A. An overview of the toxic effects of oleander in humans. Journal of Genetics and Genetic Engineering. 2019;3(3):1-5.
32. Mouhcine M., Amin L., Saaid A., Khalil H., Laila B., Mohammed E.M. Cytotoxic, antioxidant and antimicrobial activities of Nerium oleander collected in Morocco. Asian Pacific Journal of Tropical Medicine. 2019;12(1):32-37.
33. Jubair N., Rajagopal M., Chinnappan S., Abdullah N.B., Fatima A. Review on the antibacterial mechanism of plant-derived compounds against multidrug-resistant bacteria (MDR). Evidence-Based Complementary and Alternative Medicine. 2021;2021:3663315.
34. Hashemi B., Karami M. Assessment of antibacterial effect of hydro-alcoholic extract of Portulaca oleracea on the human pathogen bacteria. Journal of Sabzevar University of Medical Sciences. 2018;25(3):303-308.
35. Khajeh H., Fazeli-Nasab B., Pourshahdad A., Mirzaei A.R., Ghorbanpour M. Green-synthesized silver nanoparticles induced apoptotic cell death in CACO2 cancer cells by activating MLH1 gene expression. Scientific Reports. 2024;14(1):29601.
36. Samiei F., Fotoohiyan Z., Salehi-Sardoei A., Fazeli-Nasab B., Mirzaei A.R., Shafi N., Shameem N., Parray J.A. Progress in soil microbiome research. In: Parray J.A., editor. Progress in Soil Microbiome Research. Cham: Springer Nature Switzerland; 2024:259-302.
37. Livermore D.M. Beta-lactamases in laboratory and clinical resistance. Clinical Microbiology Reviews. 1995;8(4):557-584.
38. Khodabandeh M., Mohammadi M., Abdolsalehi M.R., Hasannejad-Bibalan M., Gholami M., Alvandimanesh A., Pournajaf A., Rajabnia R. High-level aminoglycoside resistance in Enterococcus faecalis and Enterococcus faecium; as a serious threat in hospitals. Infectious Disorders - Drug Targets. 2020;20(2):223-228.

39. Krawczyk B., Leibner J., Stojowska K., Kur J. PCR melting profile method for genotyping analysis of vancomycin-resistant Enterococcus faecium isolates from Hematological Unit patients. Polish Journal of Microbiology. 2007;56:65-70.
40. Tong S.Y., Giffard P.M. Microbiological applications of high-resolution melting analysis. Journal of Clinical Microbiology. 2012;50(11):3418-3421.
41. The UniProt Consortium. UniProt: the universal protein knowledgebase in 2021. Nucleic Acids Research. 2021;49(D1):D480-D489.
42. Haji Rastamloo B., Ziyani R., Omrani S. Biosynthesis of silver nanoparticles by using Salvia officinalis extract and evaluation of antioxidant activity and their antimicrobials against bacteria of food corruption. Journal of Food Science and Technology. 2018;11(2):108-118.
43. Nanda A., Saravanan M. Biosynthesis of silver nanoparticles from Staphylococcus aureus and its antimicrobial activity against MRSA and MRSE. Nanomedicine: Nanotechnology, Biology and Medicine. 2009;5(4):452-456.
44. Stansfield I., Jones K.M., Herbert P., Lewendon A., Shaw W.V., Tuite M.F. Missense translation errors in Saccharomyces cerevisiae. Journal of Molecular Biology. 1998;282(1):13-24.
45. Gupta K., Hooton T.M., Naber K.G., Wullt B., Colgan R., Miller L.G., Moran G.J., Nicolle L.E., Raz R., Schaeffer A.J. International clinical practice guidelines for the treatment of acute uncomplicated cystitis and pyelonephritis in women: a 2010 update by the Infectious Diseases Society of America and the European Society for Microbiology and Infectious Diseases. Clinical Infectious Diseases. 2011;52(5):e103-e120.
46. Taşlı H., Bahar I.H. Molecular characterization of TEM- and SHV-derived extended-spectrum beta-lactamases in hospital-based Enterobacteriaceae in Turkey. Japanese Journal of Infectious Diseases. 2005;58(3):162-167.
47. Bellinger C.G., Conway H. Effects of silver nitrate and sulfamylon on epithelial regeneration. Plastic and Reconstructive Surgery. 1970;45(6):582-585.
48. Bauernfeind A., Stemplinger I., Jungwirth R., Ernst S., Casellas J. Sequences of beta-lactamase genes encoding CTX-M-1 (MEN-1) and CTX-M-2 and relationship of their amino acid sequences with those of other beta-lactamases. Antimicrobial Agents and Chemotherapy. 1996;40(2):509-513.
49. Kalantar D., Mansouri S. Emergence of multiple β-lactamases produced by Escherichia coli clinical isolates from hospitalized patient in Kerman, Iran. Jundishapur Journal of Microbiology. 2010;3(4):137-145.
50. Jamil J., Haroon M., Sultan A., Khan M.A., Gul N. Prevalence, antibiotic sensitivity and phenotypic screening of ESBL/MBL producer E. coli strains isolated from urine; District Swabi, KP, Pakistan. Journal of the Pakistan Medical Association. 2018;68(11):1704-1707.
51. Soltan Dallal M.M., Aghamirzaei H.M., Mehrabadi J.F., Lari A.R., Sabbaghi A., Eshraghian M.R., Sanei A.F., Bakhtiari R., Abdar M.H. Molecular detection of TEM and AmpC (Dha, mox) broad spectrum β-lactamase in clinical isolates of Escherichia coli. Tehran University Medical Journal. 2010;68(6):315-326.
52. Melzer M., Petersen I. Mortality following bacteraemic infection caused by extended spectrum beta-lactamase (ESBL) producing E. coli compared to non-ESBL producing E. coli. Journal of Infection. 2007;55(3):254-259.
53. Fang H., Ataker F., Hedin G.R., Dornbusch K. Molecular epidemiology of extended-spectrum β-lactamases among Escherichia coli isolates collected in a Swedish hospital and its associated health care facilities from 2001 to 2006. Journal of Clinical Microbiology. 2008;46(2):707-712.
54. Shakil S., Akram M., Ali S.M., Khan A.U. Acquisition of extended-spectrum β-lactamase producing Escherichia coli strains in male and female infants admitted to a neonatal intensive care unit: molecular epidemiology and analysis of risk factors. Journal of Medical Microbiology. 2010;59(8):948-954.
55. Haddadi A. Frequency determination of blaTEM & blaSHV in the extended-spectrum beta-lactamase producing Escherichia coli isolates from Karaj. Iranian Journal of Medical Microbiology. 2017;11(2):75-80.
56. Lara H.H., Ayala-Núnez N.V., Ixtepan Turrent L.d.C., Rodríguez Padilla C. Bactericidal effect of silver nanoparticles against multidrug-resistant bacteria. World Journal of Microbiology and Biotechnology. 2010;26:615-621.
57. Quinteros M., Radice M., Gardella N., Rodriguez M., Costa N., Korbenfeld D., Couto E., Gutkind G. Extended-spectrum β-lactamases in Enterobacteriaceae in Buenos Aires, Argentina, public hospitals. Antimicrobial Agents and Chemotherapy. 2003;47(9):2864-2867.
58. Kavoosi S., Yaghoubi H. Synthesis of silver nanoparticles using green method of plant extract European marjoram (Origanum majorana) and their antibacterial effects. Cellular and Molecular Research (Iranian Journal of Biology). 2017;30(2):161-173.
59. Lee SeungJu L.S., Lee DongSup L.D., Choe HyunSop C.H., Shim BongSuk S.B., Kim ChulSung K.C., Kim MinEui K.M., Cho YongHyun C.Y. Antimicrobial resistance in community-acquired urinary tract infections: results from the Korean Antimicrobial Resistance Monitoring System. Korean Journal of Urology. 2011.
60. Mantadakis E., Tsalkidis A., Panopoulou M., Pagkalis S., Tripsianis G., Falagas M., Kartali-Ktenidou S., Chatzimichael A. Antimicrobial susceptibility of pediatric uropathogens in Thrace, Greece. International Urology and Nephrology. 2011;43:549-555.
61. Ghaderi R.S., Kazemi M., Soleimanpour S. Nanoparticles are more successful competitor than antibiotics in treating bacterial infections: a review of the literature. Iranian Journal of Medical Microbiology. 2021;15(1):18-45.
62. Calderón-Jiménez B., Johnson M.E., Montoro Bustos A.R., Murphy K.E., Winchester M.R., Vega Baudrit J.R. Silver nanoparticles: technological advances, societal impacts, and metrological challenges. Frontiers in Chemistry. 2017;5:6.
63. Song J.Y., Kim B.S. Rapid biological synthesis of silver nanoparticles using plant leaf extracts. Bioprocess and Biosystems Engineering. 2009;32(1):79-84.
64. Tomaszewska E., Soliwoda K., Kadzioła K., Tkacz-Szczęsna B., Celichowski G., Cichomski M., Szmaja W., Grobelny J. Detection limits of DLS and UV-Vis spectroscopy in characterization of polydisperse nanoparticles colloids. Journal of Nanomaterials. 2013;2013:313081.
65. Tabatabaei Yazdi F., Alizadeh Behbahani B., Heidari Sureshjani M., Mortazavi S.A. The in vitro study of antimicrobial effect of Teucrium polium extract on infectious microorganisms. Avicenna Journal of Clinical Medicine. 2014;21(1):16-24.
66. Khalil M.M.H., Ismail E.H., El-Baghdady K.Z., Mohamed D. Green synthesis of silver nanoparticles using olive leaf extract and its antibacterial activity. Arabian Journal of Chemistry. 2014;7(6):1131-1139.
67. Patra J.K., Baek K.H. Biosynthesis of silver nanoparticles using aqueous extract of silky hairs of corn and investigation of its antibacterial and anticandidal synergistic activity and antioxidant potential. IET Nanobiotechnology. 2016;10(5):326-333.
68. Kvítek L., Panáček A., Soukupová J., Kolář M., Večeřová R., Prucek R., Holecová M., Zbořil R. Effect of surfactants and polymers on stability and antibacterial activity of silver nanoparticles (NPs). The Journal of Physical Chemistry C. 2008;112(15):5825-5834.
69. Savithramma N., Rao M.L., Rukmini K., Devi P.S. Antimicrobial activity of silver nanoparticles synthesized by using medicinal plants. International Journal of ChemTech Research. 2011;3(3):1394-1402.
70. Morones J.R., Elechiguerra J.L., Camacho A., Holt K., Kouri J.B., Ramírez J.T., Yacaman M.J. The bactericidal effect of silver nanoparticles. Nanotechnology. 2005;16(10):2346.
71. Li W.-R., Xie X.-B., Shi Q.-S., Duan S.-S., Ouyang Y.-S., Chen Y.-B. Antibacterial effect of silver nanoparticles on Staphylococcus aureus. BioMetals. 2011;24(1):135-141.
72. Vijayakumar M., Priya K., Nancy F., Noorlidah A., Ahmed A. Biosynthesis, characterisation and anti-bacterial effect of plant-mediated silver nanoparticles using Artemisia nilagirica. Industrial Crops and Products. 2013;41:235-240.

73. Mohasseli T. Green synthesis and characterization of silver nanoparticles using aqueous extract of Sesamum indicum seeds. Modares Journal of Biotechnology. 2015;6(1):10-20.
74. Rezaee P., Kermanshahi K. The antimicrobial effect of chitosan nanoparticles film on two species of food bacteria. Journal of Food Technology and Nutrition. 2015;3(12):5-12.
75. Sondi I., Salopek-Sondi B. Silver nanoparticles as antimicrobial agent: a case study on E. coli as a model for Gram-negative bacteria. Journal of Colloid and Interface Science. 2004;275(1):177-182.
76. Rashid A., Molavi F., Mahmoudzadeh H. The effect of silver nanoparticles on mecA gene expression in methicillin-resistant samples of Staphylococcus aureus. New Cellular and Molecular Biotechnology Journal. 2020;11(41):67-82.
77. Rashid A., Molavi F., Mahmoudzadeh H. The effect of silver nanoparticles on mecA gene expression in methicillin-resistant samples of Staphylococcus aureus. New Cellular and Molecular Biotechnology Journal. 2020;11(41):67-82.
78. Chaudhari P.R., Masurkar S.A., Shidore V.B., Kamble S.P. Effect of biosynthesized silver nanoparticles on Staphylococcus aureus biofilm quenching and prevention of biofilm formation. Nano-Micro Letters. 2012;4:34-39.
79. Piri Gharaghie T., Sadat Shandiz S.A. The inhibitory effects of silver nanoparticles on bap gene expression in antibiotic-resistant Acinetobacter baumannii isolates using real-time PCR. Journal of Ilam University of Medical Sciences. 2018;26(4):175-185.